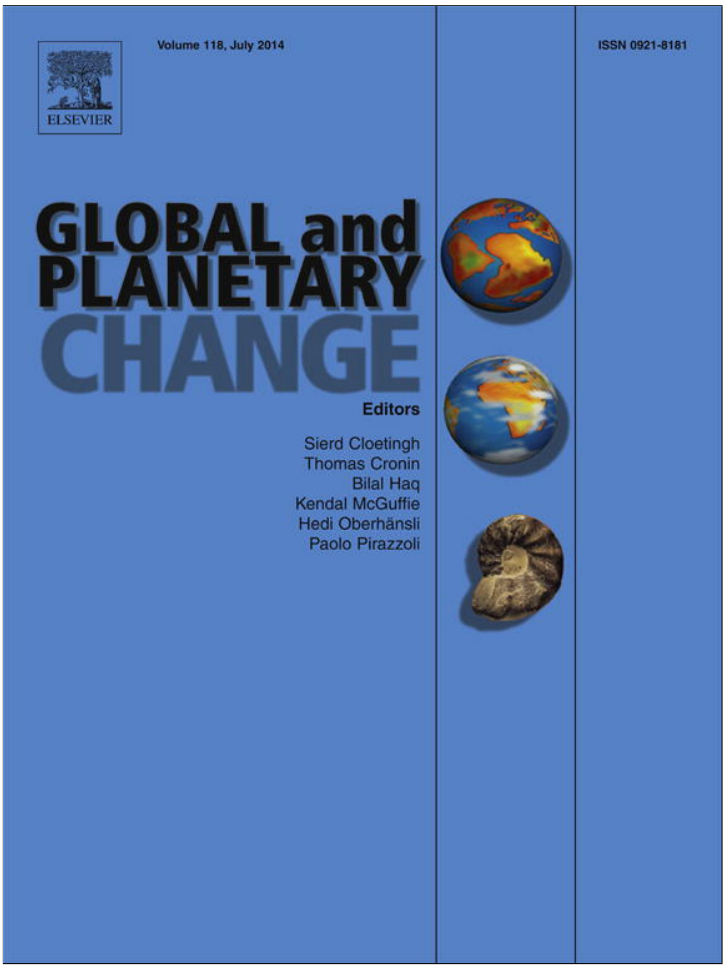

Global and Planetary Change 118 (2014) 16–24

Contents lists available at ScienceDirect

Global and Planetary Change

journal homepage: www.elsevier.com/locate/gloplacha

Emplacement of Antarctic ice sheet mass affects circumpolar ocean flow

Maria Rugenstein [a,*], Paolo Stocchi [b], Anna von der Heydt [a], Henk Dijkstra [a], Henk Brinkhuis [b]

[a] Institute for Marine and Atmospheric Research Utrecht Center for Extreme Matter and Emergent Phenomena, Utrecht University, Utrecht, The Netherlands
[b] NIOZ, Royal Netherlands Institute for Sea Research, Den Burg, The Netherlands

ARTICLE INFO

Article history:
Received 7 December 2013
Received in revised form 22 March 2014
Accepted 24 March 2014
Available online 5 April 2014

Keywords:
Antarctic ice sheet
Ice load
Southern Ocean
Eocene–Oligocene
Frontal shifts

ABSTRACT

During the Cenozoic the Antarctic continent experienced large fluctuations in ice-sheet volume. We investigate the effects of Glacial Isostatic Adjustment (GIA) on Southern Ocean circulation for the first continental scale glaciation of Antarctica (~34 Myr) by combining solid Earth and ocean dynamic modeling. A newly compiled global early Oligocene topography is used to run a solid Earth model forced by a growing Antarctic ice sheet. A regional Southern Ocean zonal isopycnal adiabatic ocean model is run under ice-free and fully glaciated (GIA) conditions. We find that GIA-induced deformations of the sea bottom on the order of 50 m are large enough to affect the pressure and density variations driving the ocean flow around Antarctica. Throughout the Southern Ocean, frontal patterns are shifted several degrees, velocity changes are regionally more than 100%, and the zonal transport decreases in mean and variability. The model analysis suggests that GIA induced ocean flow variations alone could impact local nutrient variability, erosion and sedimentation rates, or ocean heat transport. These effects may be large enough to require consideration when interpreting the results of Southern Ocean sediment cores.

1. Motivation

At the Eocene–Oligocene boundary ~33 million years ago (Myr), the Southern Hemispheric climate system experienced a rapid transition. The quasi ice-free Antarctic continent glaciated within less than $5 \cdot 10^5$ years, oscillated in orbitally paced glacial cycles between 40% and 140% of its present day volume for about ten million years, almost vanished at the Oligocene–Miocene boundary (23 Myr), but increased again in the mid to late Miocene (Hambrey et al., 1991; Zachos et al., 1997; DeConto et al., 2008; Gallagher et al., 2013). Simultaneously, in between the late Eocene and the early Miocene, the Southern Ocean circulation reorganized from basin wide gyres to an Antarctic Circumpolar Current (ACC). The development of the (proto) ACC was facilitated by the opening of two gateways: (1) the well-constrained deepening of the Tasmanian Gateway at 33.5 Myr (Stickley et al., 2004; Bijl et al., 2013), and (2) the Drake Passage, which opened/deepened sometime between 41 and 23 Myr (e.g. Barker and Burrell, 1977; Scher and Martin, 2006; Dalziel et al., 2013).

Two hypotheses have been proposed for the sudden glaciation of Antarctica at the end of the Eocene: ice sheet growth dominantly controlled by (1) the thermal isolation of the continent through the development of the ACC or (2) global cooling due to CO_2 changes (Kennett, 1977; Oglesby, 1989). Previous model studies have focused on either or both of these mechanisms, which involve ocean–atmosphere, atmosphere–ice sheet or ice sheet–bedrock interactions (e.g. Huber and Nof, 2006; DeConto et al., 2008; Sijp and England, 2011; Cristini et al., 2012; Lefebvre et al., 2012; Yang et al., 2013). Other mechanisms proposed to have influenced ice sheet growth are transitions of the Atlantic meridional overturning circulation (Tigchelaar et al., 2011) or the shallow opening of the Tasman Gateway, which might have cooled the Antarctic margins and waters of intermediate depth (Bijl et al., 2013).

The Antarctic ice sheet today stores approximately $25 \cdot 10^6$ km^3 of water, while the highest estimates for the early Oligocene are $36 \cdot 10^6$ km^3 (Wilson et al., 2013). The load exerted on the solid Earth surface and the gravitational pull exerted by the growing ice sheet on the oceans result in space- and time-dependent deformations of the crust and of the mean sea surface, the latter remaining an equipotential surface of gravity (Farrell and Clark, 1976). Known as Glacial Isostatic Adjustment, the combination of these processes are accounted for by solving the Sea Level Equation (SLE) for a prescribed ice sheet chronology and solid Earth rheological model (Spada and Stocchi, 2007). Since the equations of ocean motion are defined relative to an equipotential surface of gravity, only a deformation of the solid Earth and a change in the water column height have the potential to impact the modeled ocean flow.

In this paper, we address the question to what extent the sea bottom deformations – induced by the Antarctic ice sheet mass – could have impacted the ocean flow in an Eocene–Oligocene–Miocene world. We focus solely on the effect of the load and mass – which has not been studied before – and thereby isolate the problem from effects of ocean

* Corresponding author.
E-mail address: maria.rugenstein@env.ethz.ch (M. Rugenstein).

http://dx.doi.org/10.1016/j.gloplacha.2014.03.011
0921-8181/

and atmospheric buoyancy and heat transport. Here, we combine for the first time a solid Earth model and an ocean model for deep-time paleo conditions. A global early Oligocene topography (described in Section 2.1) is used to run a solid Earth model (Section 2.2) forced by a growing Antarctic ice sheet. Subsequently, a zonal isopycnal adiabatic ocean model (Section 2.3) representing the Southern Ocean is forced with the ice free topography and the ice load adjusted topography. Results of the simulations are presented in Section 3. Analysis of ocean model output in terms of the vertically integrated vorticity equation is presented in Section 4. Before we conclude in Section 6, we discuss possible implications of our findings and their relation to proxy measures in Section 5.

2. Model setup and experimental design

2.1. Reconstruction of early Oligocene topography

We compiled a global early Oligocene topography from different datasets (Fig. 1). Markwick et al. (2000) is used for the continental shape and topography, Wilson et al. (2012) for the Antarctic topography, and Müller et al. (2008) for the deep sea bathymetry. The shelf and coast areas are interpolated between these datasets (Somme et al., 2009), dependent upon how much is known for a region (e.g., Close et al., 2009, for the continental margin along Wilkes Land). Poorly constrained regions were supplemented or adapted with data from: Meulenkamp and Sissingh (2003) for the Tethys region, van Hinsbergen et al. (2012) and Torsvik et al. (2012) for the Indian–South Asian region and the position of Africa and South America, McQuarrie and van Hinsbergen (2013) for the Arabian region, and Mix et al. (2011) for the elevation of Western North America. We used the program GPlates (http://www.gplates.org/) to assure the relative position of the continental plates; where they differ from the Markwick data set the GPlate position was prioritized. The reconstruction has a resolution of 1° and is available (together with a vegetation file not used here) in different configurations for the Southern Ocean gateways upon request from the authors. It is more realistic, detailed and has a higher resolution than those used in earlier modeling studies for the Eocene or Oligocene time periods (e.g. Huber and Nof, 2006; Sijp and England, 2011; Cristini et al., 2012).

For this study we interpolated the topography to 1/4° resolution and both Southern Ocean gateways are assumed to be open and deep. The timing of the Drake Passage opening and deepening is widely debated (Diester-Haass and Zahn, 1996; Latimer and Filippelli, 2002; Lawver and Gahagan, 2003; Barker and Thomas, 2004; Livermore et al., 2005; Pfuhl and McCave, 2005; Dalziel et al., 2013). Due to these considerable uncertainties, our configuration can be representative of the late Eocene, Oligocene, or possibly the Miocene. Thus, we use the Eocene–Oligocene transition as an *example* of a time slice where the Southern Ocean gateways were deep and the Antarctic ice volume changed substantially. We are concerned with the mechanism that connects changing ice load and changing ocean depth, and do not attempt to explain the temporal behavior of specific proxies. The choice of deep gateways is discussed further in Sections 2.3 and 5.

2.2. Solid Earth model and sea level equation

We use the code SELEN (Spada and Stocchi, 2007) to solve the SLE by means of the pseudo-spectral method (Mitrovica and Peltier, 1991) and retrieve the relative sea level changes on a global scale and in time. We assume that the Earth is spherically symmetric, self-gravitating, non-rotating, and radially stratified. Hence, the rheological parameters only depend upon the distance from the center of mass of the Earth and no lateral variations are accounted for. The outer shell is assumed to be perfectly elastic and mimics the lithosphere. The mantle is discretized into three Maxwell viscoelastic layers, the inner core is assumed to be inviscid. We adopt the normal mode technique to generate the response of the Earth to variations of surface ice- and water-loading (Peltier, 1974). We solve the SLE for the viscous and elastic components of the solid Earth deformation by simulating the ice-sheet chronology over 2.2 Myr. Fig. 2 shows the global relative sea level change (left column) and that of a sector around Antarctica (right column) at 1.5 (a,b), 1.55 (c,d), and 2.2 Myr (e,f).

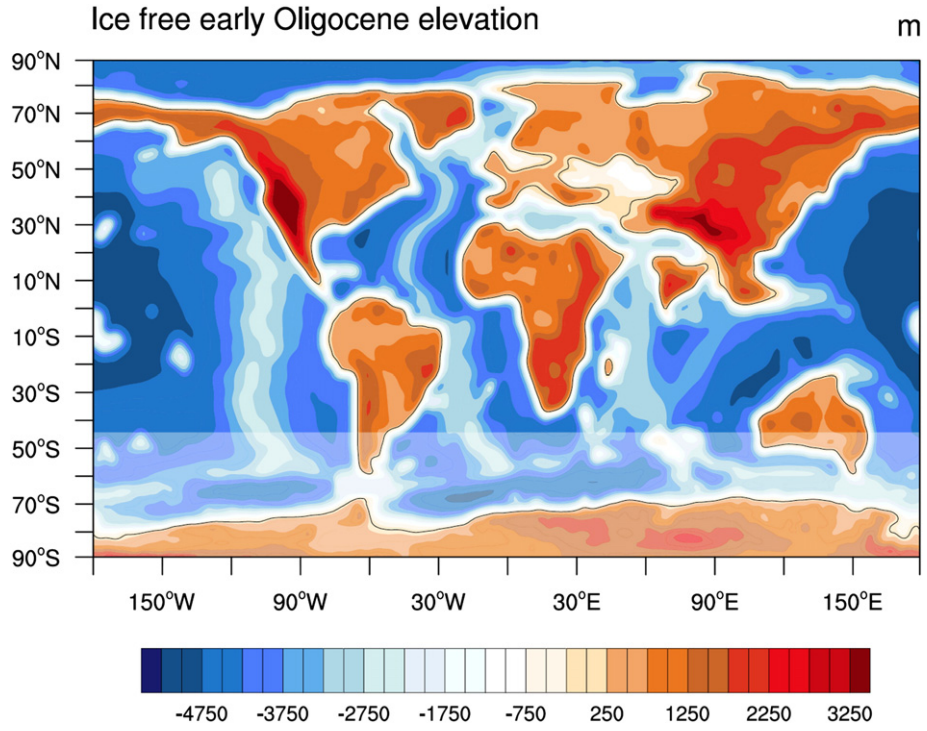

Fig. 1. Ice free global topography used to initiate the solid Earth model. The shaded part is the region used for the ocean model control run. The dataset is available upon request for different versions of Southern Ocean gateways.

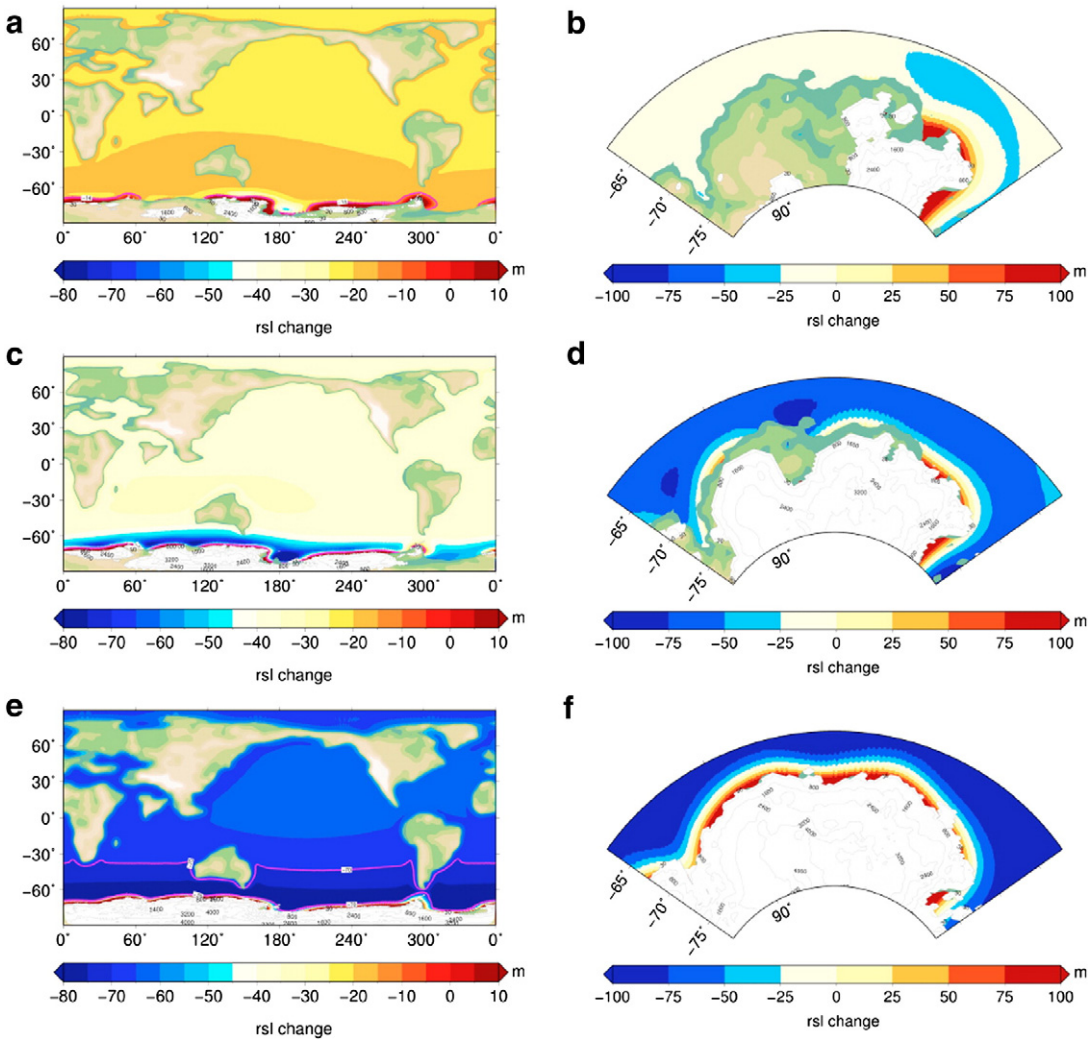

Fig. 2. Relative sea level change simulated by solving the sea level equation under Eocene–Oligocene ice sheet chronology and the topography of Fig. 1. Global (left) versus regional (right) view for model run time of 1.5 (a,b), 1.55 (c,d), and 2.2 Myr (e,f). The eustatic sea level drop is 14, 38, and 70 m respectively.

The relative sea level change includes the crustal deformation and the change in the water column height. During the buildup of the ice sheet the relative sea level height has a strong spatial dependence. After a 2.2 Myr model run time (100 kyr after the full formation of the ice sheet) the crustal deformation is in quasi-equilibrium, while the water column height can be approximated by the eustatic (global uniform) solution (see Fig. 2e).

The final relative sea level change depends on the way the ice load is applied in time. Instead of an instantaneously emplaced ice load, we choose a more realistic situation with the ice sheet growing in time. The final ocean model results are sensitive to the choice of ice sheet shape and growth in their *spatial* structure, but not in the overall response to the ice sheet load (see Section 3). We chose an intermediate final ice volume of $30 \cdot 10^6$ km^3, which results in an eustatic sea-level drop of ~70 m (Stocchi et al., 2013; Wilson et al., 2013).

Fig. 3a shows the difference between the control and GIA-induced solid Earth deformation.[1] Directly around the ice sheet the sea floor is depressed, whereas a bulge of up to 70 m forms around the continent and the remainder of Southern Ocean sea floor is raised nearly homogeneously.

2.3. Ocean model

We use the two-layer version of the Hallberg Isopycnal Model (HIM) to study flows in the Southern Ocean under different bathymetries, sketched in Fig. 3b. HIM solves the hydrostatic primitive equations using a split barotropic/baroclinic time-stepping scheme, conserving the mass of each layer when no diapycnal mixing parameterization is applied (Hallberg, 1997). The model is used adiabatically with a Laplacian along-isopycnal viscosity of 50 m^2/s (Griffies and Hallberg, 2000). Sensitivity runs with other viscosities are discussed in Appendix A.

The two layers mimic the thermocline/upper layer and the deep ocean with densities of 1030 and 1032 kg/m^3 and equilibrium depths of 1 and 4 km, respectively. In the horizontal the resolution is eddy permitting 0.25° × 0.25° in longitude and latitude. The sensitivity of the results to the horizontal resolution is discussed in Section 3 and the Appendix A. The spatial domain spans the Southern Ocean with the Antarctic coast line as the southern boundary and a rigid (undamped) no-slip northern boundary at 45°S (shaded area in Fig. 1). A steady, zonally constant wind-stress forcing with a maximum of 0.15 Pa at 52°S is prescribed at the surface and the densities of the layers are chosen such that an ACC transport of about 125 Sv results (Fig. 3b). We choose present-day values of wind stress and ACC strength because both values

[1] The solid Earth deformation is the same as the crustal deformation, also called *vertical displacement* term in the SLE, i.e. relative sea level change minus water column height change. In the ocean model context – with the reference frame of the equipotential surface equaling the undisturbed global average sea surface height – it is the same as the difference of bottom boundary conditions for our two simulations.

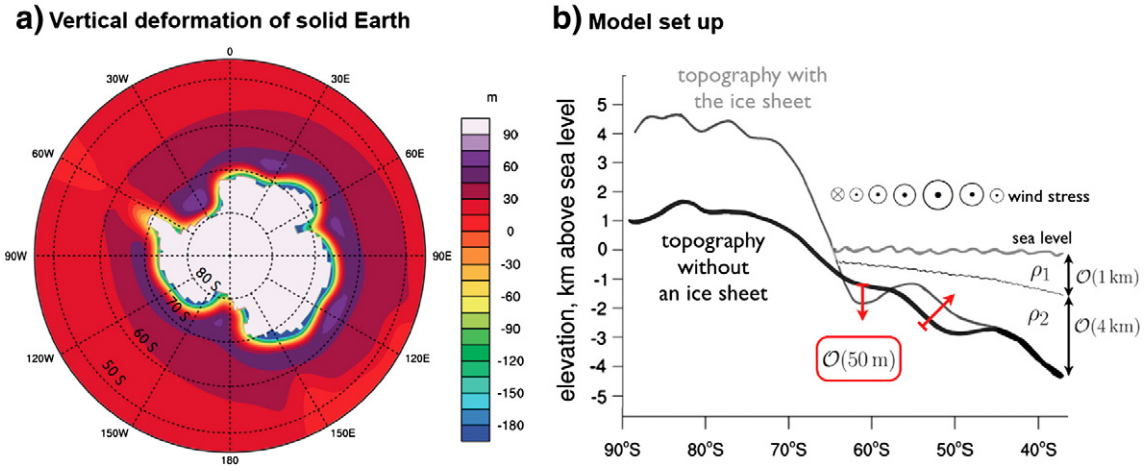

Fig. 3. (a) Solid Earth response to the ice sheet loading (m above sea level): GIA case minus control case bathymetry. (b) Sketch to illustrate the model set up: imaginary zonal section with the control case topography in thick black and the GIA adjusted topography plus ice sheet in thinner gray. The westerly wind strength maximum is at 52°S and the layers of the ocean model are indicated.

are unknown for the Eocene to Miocene time (see also discussion in Section 5). We run the ocean model once with the ice free topography (hereafter control run) and once with the GIA-equilibrated topography (hereafter GIA run). To assure mass conservation of the whole system, we reduce the upper ocean layer height in the GIA run, accounting for the 70 m eustatic sea level drop resulting from the emplacement of the ice sheet by evaporated ocean water. In Fig. 5 we also show the solution for the alternative, but less physically motivated, choice of lower layer depth reduction. We do not include lateral gradients of gravity in the ocean model to account for the higher sea level around the ice sheet induced by gravitational attraction of the ice mass (Fig. 2e). After 2.2 Myr, this effect is less than 2% of the sea bottom deformation (compare Fig. 3a with Fig. 2e).

3. Results

In the following, we compare the two equilibrated ocean simulations (control and GIA). All plotted fields are 25 year averages following a spin up of 120 years. The mean flow of the control case (Fig. 4a and c) is overall eastward and strong frontal patterns can be seen, e.g. south of Australia. Locally velocities reach up to 1.5 m/s, but are mostly within 0.1 to 0.3 m/s, which compares well to today's ACC velocities (Zambianchi et al., 1999). Since the Drake Passage width is similar to modern times but lies farther South (≈68°–60°S in Oligocene compared to 63°–55°S today), a gyre like structure forms to its west. The spatial positions of the fronts are sensitive to the prescribed depth of Drake Passage (2 km) and Tasman Seaway (2.5 km) and the stratification. Fig. 4b and d shows the zonal and meridional velocity difference (GIA–control run). The velocity amplitude changes up to more than 0.2 m/s, locally more than 100% of the control run flow. Most prominently, the zonal frontal pattern between Australia and the coast of Antarctica shifts approximately 2° north. The lower layer velocity amplitudes (not shown) are an order of magnitude smaller, but retain patterns of frontal shifts expressed in the upper layer. The spatial pattern of the velocity field of the control case and the difference field between GIA and control cases is robust with respect to the horizontal resolution investigated (not shown).

Fig. 5 shows the change of the zonal transport through Drake Passage, with the control run (125 Sv on average) and the GIA run (110 Sv on average). The ocean model flow is statistically stationary and the mean zonal transport is the same at every longitude, while the variance – caused by mixed barotropic/baroclinic instabilities – differs from place to place. Through Drake Passage, the variance is reduced by 78% in the GIA run compared with the control and the total transport decreases 12% or 15 Sv, which is made up by volume reduction as well as dynamical response to the new bathymetry and sea level.

To test the relative contribution of volume reduction and dynamical response, we analyze two additional sensitivity runs. In the case referred to as (*LL-GIA*) (with a mean transport of 117 Sv, depicted in orange) the water for the ice sheet is taken out of the lower layer. The combination of dynamic and volume change response is in this case around 7 Sv. In the case referred to as (*N-GIA*), no depth reduction at all (with a mean transport of 118 Sv, depicted in yellow) is considered, meaning the water which forms the ice-sheet is "extra-terrestrial". This implies that the overall mass is not conserved since the solid Earth model is still run under the assumption of ocean load including 70 m of eustatic sea level drop. The response is in this case only due to dynamical reasons, and its mean is equal to 7 Sv. Both cases (*LL-GIA*) and (*N-GIA*) show very similar velocity response patterns as the GIA case in Fig. 4.

While in the GIA case (red) the upper layer makes up the major part of the total (volume + dynamic) transport reduction (~12 of 15 Sv). From the LL-GIA case, we can deduce that about 7 Sv of this reduction can be attributed to dynamic influences (e.g. changes in the bathymetry) and hence the remaining part is due to volume changes. This is in agreement with a rough estimate of this contribution based on the width of Drake Passage (800 km), the change in depth (70 m) and the average velocity in Drake Passage (0.1 m/s), which is about 6 Sv. Note that in the (*LL-GIA*) case, the volume contribution is relatively small because the velocities in the lower layer are much smaller than those in the upper layer.

The blue and red bars in Fig. 5 represent two standard deviations of the zonal transport through Drake Passage, indicating that not only the mean zonal transport but also the variability of the transport changes. Fig. 6 shows a more complete picture providing the standard deviation of the velocity amplitude for each grid point for the control run (panel a) and GIA–control run (panel b). The variance of the flow changes depends on the local relative – upper versus lower – layer height change by (1) the solid earth ice load adjustment, (2) the volume reduction/ice mass build up, and (3) the local dynamic response and propagation of barotropic/baroclinic instabilities. The Rossby deformation radius decreases with decreasing layer depth, thus, eddies are less well resolved for a smaller layer height. See Table A.1 for more details on each case. Fig. 6 shows that the variance increases or decreases regionally more than 100% (e.g. East/West of 150°E). Combining Figs. 6b, 4b and

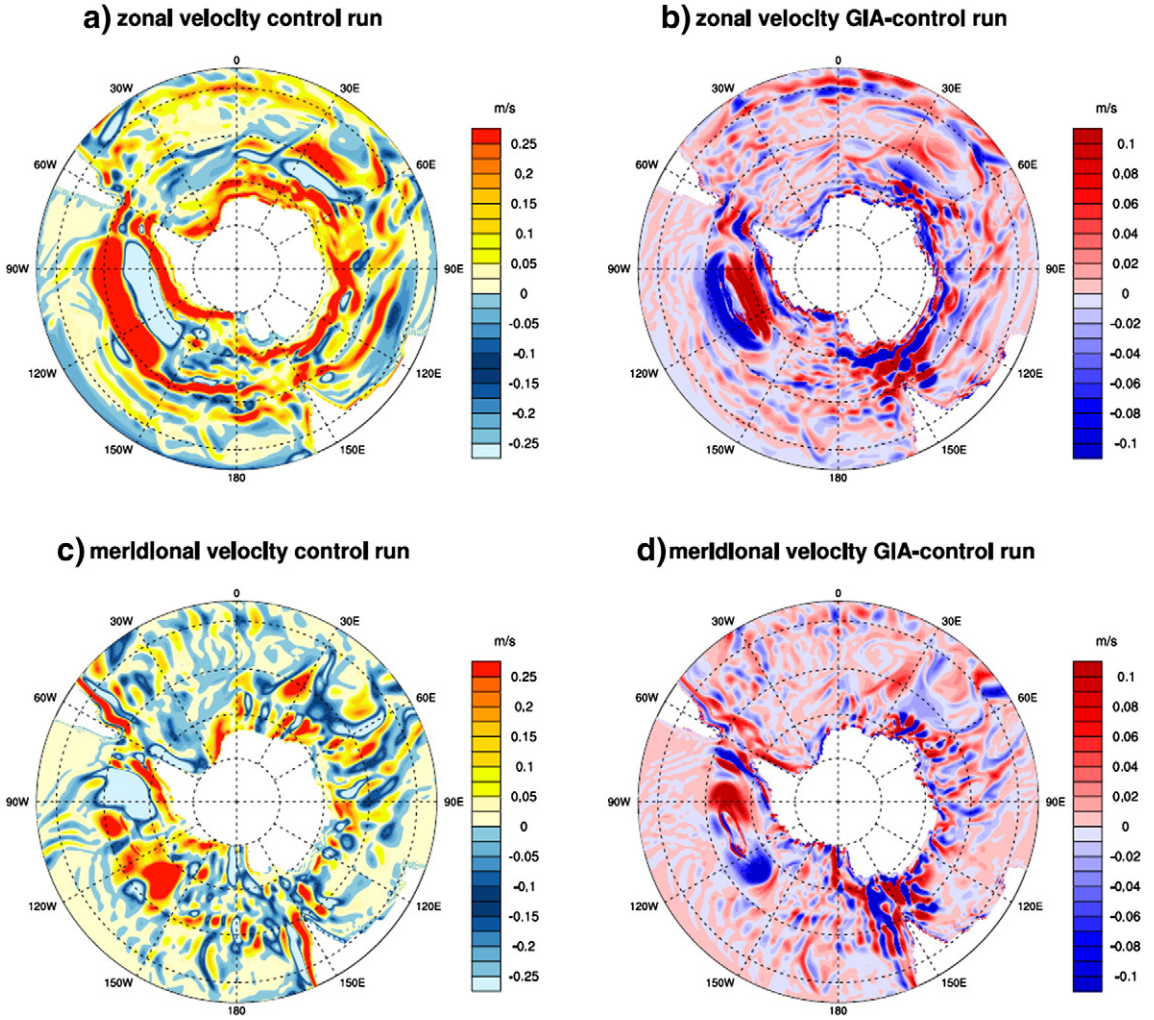

Fig. 4. Zonal (a and b) and meridional (c and d) velocities of the upper layer control run (left) and GIA–control run (right) in m/s.

d for a certain location e.g. IODP site U1356 at ~148°E 68°S (see also Bijl et al., 2013) indicates how the paths of passive tracers could change locally. The mean meridional velocity component becomes stronger in magnitude across the whole meridional domain, while the (strongly) reduced variance implies a changed eddy field. Possible consequences are discussed in Section 5. So far, we can conclude that the load of the Antarctic ice sheet as pure load but also as mass redistribution from the ocean to the land changes regional circulation strength, pattern, and variability throughout the Southern Ocean in this model.

4. Analysis

To interpret the flow differences between the control and GIA case, we analyze the depth integrated vorticity equation. Here, we

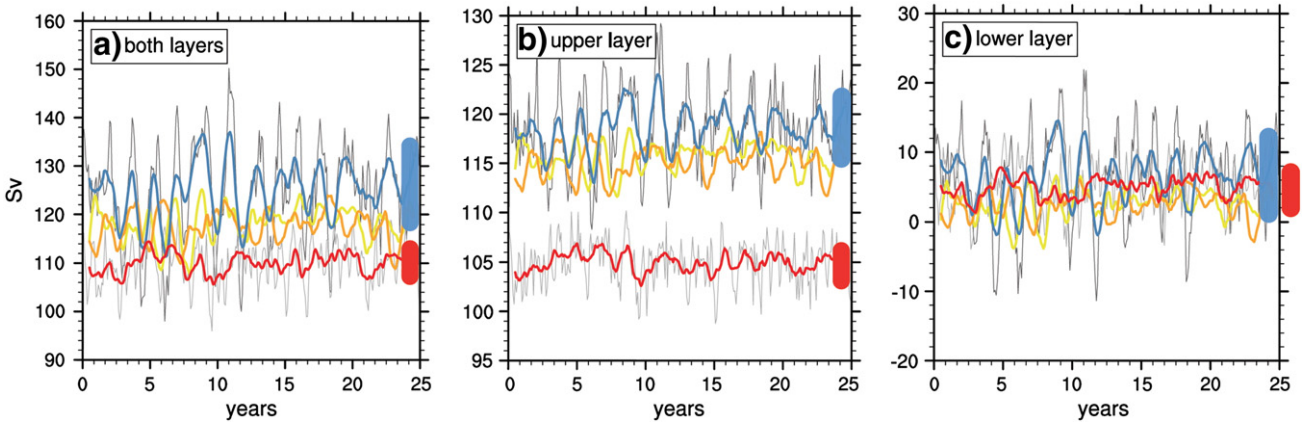

Fig. 5. 25 year time series of one year running mean of the zonal transport (Sv) through Drake Passage. Control run in blue (full time series in black) and GIA run in red (full time series in gray) with two standard deviations depicted as bar on the right side. Mass removal from lower layer in orange, and non-mass conservation run in yellow.

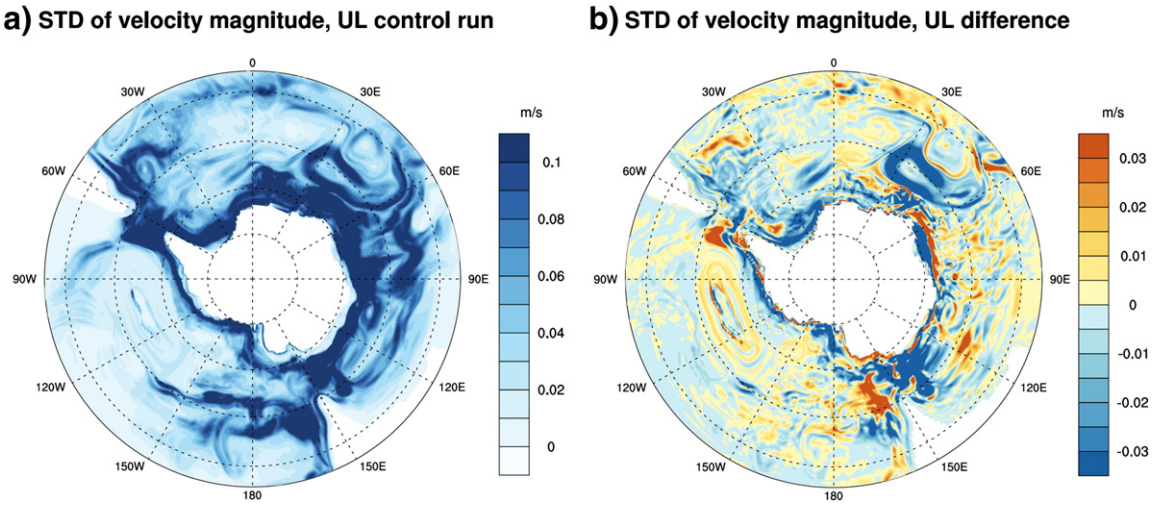

Fig. 6. Standard deviation of the velocity magnitude for the upper layer control run (a) and the GIA–control run (b) in m/s.

use the more transparent Cartesian form, whereas HIM uses spherical coordinates.

$$\overline{\mathbf{u}} \cdot \nabla \frac{f}{H} = \frac{1}{H^2}\left(\frac{\partial \chi}{\partial y}\frac{\partial H}{\partial x} - \frac{\partial \chi}{\partial x}\frac{\partial H}{\partial y}\right) - \frac{\partial}{\partial y}\left(\frac{\tau^x}{H\rho_0}\right) + R, \tag{1}$$

where $\overline{\mathbf{u}} = h_1\overline{\mathbf{u}}_1 + h_2\overline{\mathbf{u}}_2$ is the vertically integrated velocity, f is the latitudinally dependent Coriolis parameter, $H = h_1 + h_2$ is the sum of the layer depths and

$$\chi = \int \frac{z}{\rho_0}\frac{\partial p}{\partial z}\mathrm{d}z \tag{2}$$

is a measure of the vertically integrated potential energy. Furthermore, τ^x is the zonal wind stress, ρ_0 is a reference density, and eddy vorticity fluxes and effects of friction are taken together in the residual term R (e.g. Olbers et al., 2004).

The first term on the right hand side of Eq. (1) represents the Joint Effect of Baroclinicity and Relief (JEBAR, henceforth J). As far as we know, this concept, introduced by Sarkisyan and Ivanov (1971), has not yet been applied to paleoceanographic flows. Depending upon its derivation, it can be regarded as the torque driving the depth averaged flow, as a frictional analogue, or – as used here – as a geostrophic correction term due to topographic stretching if one uses depth averaged velocities instead of bottom velocities (Mertz and Wright, 1992; Cane et al., 1998).

In a homogeneous and unforced ocean, the J term would be zero and the flow would follow geostrophic contours (curves of constant f/H). In a stratified eddying ocean, the energy input by the wind is thought to be transferred downwards by eddy form stresses between the layers and dissipated by bottom form stress. In our formulation with two layers, χ is thus nonzero and the J together with the R terms balance the left hand side of Eq. (1), while the wind stress is one to two orders of magnitude smaller. Fig. 7 shows the 25 year time average left hand

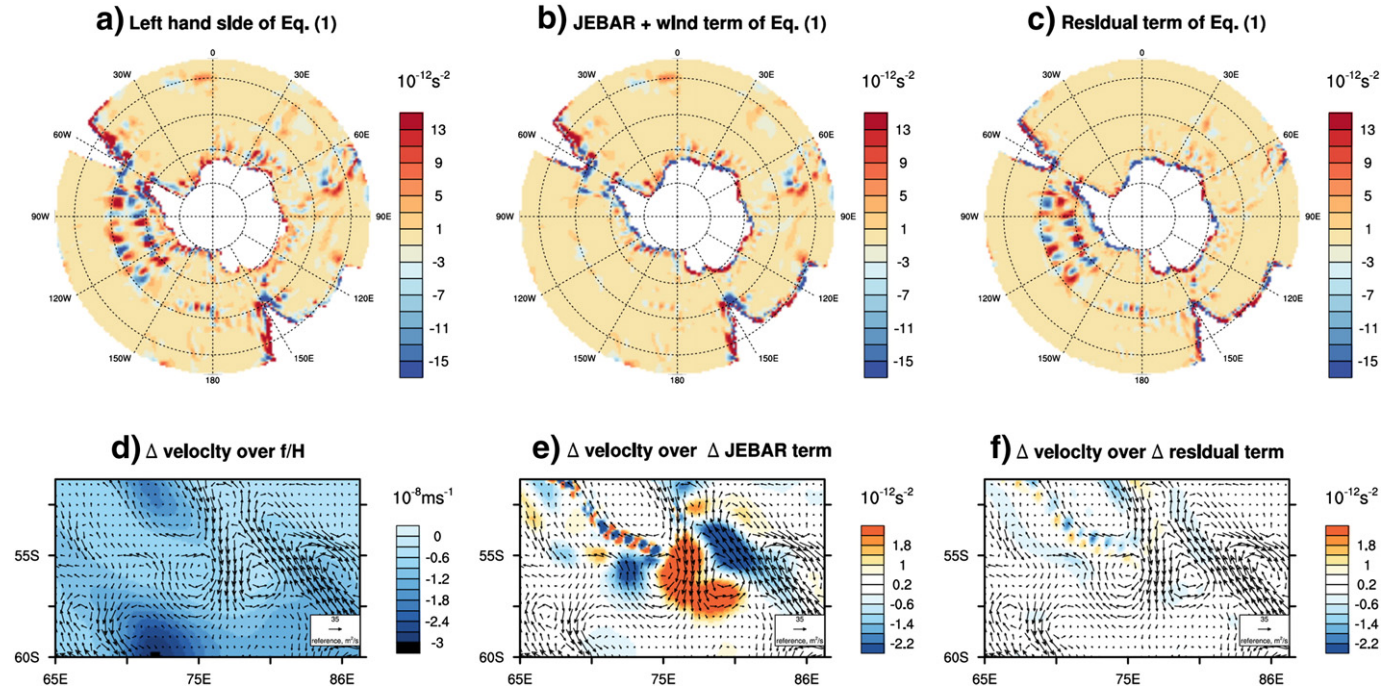

Fig. 7. Terms in the vertically integrated vorticity equation of the control run (in 10^{-12} s^{-2}, a–c). Close up of one region with the GIA–control run *velocity difference vector field* over the difference in f/H contours (d), the JEBAR term (e), the residual term (f).

side of Eq. (1) (panel a), the wind plus dominating J term (b), and the R term (c). The main JEBAR contribution appears to result from the slopes, with a positive (negative) J term above $\partial H/\partial\chi \ll 0 (\gg 0)$, while the R term is comparably large inside the gyre (eddy vorticity flux) and along the coasts (effects of friction). In conditions with less eddies (higher viscosity see Appendix A) the response of the residual term is confined to the region around the coast and considerable smaller than the J term. With a changing bathymetry and possibly changing sea level height – thus the relative contribution of h_1 and h_2 to H – both sides of Eq. (1) change.

To decompose the relation between the terms in the vorticity equation and the changing flow field we zoom into one region (65°–88°E and 62–50°S), with a sill and small R term facilitating the analysis. Fig. 7d–f shows the GIA–control run velocity difference vector field over the difference in geostrophic (f/H) contours (d), the J term (e), and the R term (f). The f/H contours move north, and without any JEBAR effect the vorticity equation shows that the flow would be approximately along these geostrophic contours. Contrary, assuming that f/H remains the same, the difference velocity field $\Delta\mathbf{u}$ can be written as $\Delta\mathbf{u} \cdot \nabla(f/H)$ $prox\Delta J$, and indicates the location where the streamlines cross the f/H contours (panel e). Considering both contributions, the total response of the ocean flow is composed out of a shift of the velocities following f/H contours (Fig. 7d) and modulated by the changing strength and location of the flow illustrated by the J term (Fig. 7e).

5. Discussion and implications

In the following we discuss time constraints and the uncertainty of the representation of the topography. We link our finding to proxy measures and suggest in which directions further research could follow up.

We stress that the mechanism proposed here holds for all continental configurations with large ice volume fluctuations on Antarctica and open and deep Southern Ocean gateways. Our estimates of possible flow change can be interpreted as conservative for the Eocene–Oligocene transition since shallow gateways and a weak ACC might be impacted even more. As an extreme case one can think of a shallow Drake Passage which – through the bulge – gets too shallow to allow closing circumpolar f/H contours and would turn a (weak proto-) ACC back into gyre flow.

Not only can growing or melting ice sheets cause the sea bottom deformations on the order of magnitude found here (about 50 m), but also continental shifts of a few degrees (Conrad, 2013). This further implies that our global topography compilation can be representative of the late Eocene, Oligocene, or even Miocene (when Australia would be located farther north). The topography used is a best guess based on most current data available but it is still very (hardly quantifiable) uncertain. However, the mechanism shown here does depend on the change of bathymetry which our model suggests is robust.

For the modern Southern Ocean, location and intensity of ACC fronts and the path of the meanders is widely discussed to impact mixing, nutrient availability, heat transport, and carbon uptake (e.g. Smith et al., 1996; Jr and Robinson, 1997; Sokolov and Rintoul, 2007; Ito et al., 2010; Graham et al., 2012; Spence et al., 2012).

For the time frame discussed here, however, quantification of these relations is even more difficult. One way is to relate increasing diatom productivity during the EOT to changing ocean circulation, usually assumed to be the spin-up of the (proto) ACC (Egan et al., 2013). Here, we show that also simply the emplacement of an ice sheet with an already existing ACC could have played a role in (possibly only local) changing eddy field, mixing, and thus nutrient availability. Next to organic productivity one might look at more direct proxies for flow pattern changes such as contourite depositional systems (Hernández-Molina et al., 2009, for the Argentinian slope from EOT onwards), or anisotropy of magnetic susceptibility and mass accumulation rate of terrigenous sediments as a proxy for the current strength (Hassold et al., 2009, for the Antarctic peninsula from late Miocene onwards). Also, the appearance of glauconite in the sediments together with sedimentary winnowing and condensation has been interpreted as invigorated bottom water circulation (Sluijs et al., 2003; Stickley et al., 2004, for the Tasman Region in the late Eocene).

A more global focus is taken by Heinze and Crowley (1997), who show in a sentiment enabled circulation model why internal reorganizations of the ocean circulation induced by gateways changes could have caused comparable responses in the geological record as air temperature, sea level, and weathering. Given these rather speculative ideas on how changing velocities are reflected in different proxies we, at this time, only suggest that researchers consider potential GIA-induced ocean flow adjustment when analyzing sediment records. However, we do not imply which specific proxies would be sensitive to these changes. Because we have used an adiabatic two-layer ocean model, we cannot determine how heat transport, stratification, or sea surface temperature change. Adapted heat transport, stratification, or thermohaline circulation might modulate or counteract the GIA effect shown here.

Previous modeling work (e.g. Oglesby, 1989 or Goldner et al., 2013) has investigated the impact of the elevated topography, temperature, and/or atmospheric circulation pattern around the expanding Antarctic Ice Sheet. Here, we have isolated the so far overlooked impact of the ice sheet mass and *load* on the Southern Ocean bathymetry and flow. Inclusion of oceanic and atmospheric buoyancy and heat transport are required to fully test the impacts of the ice sheet load effect shown here.

We speculate that, if sea surface temperatures change enough to impact evaporation patterns and moisture transport towards the inner Antarctic continent a feedback process of ice growth could take place (Prentice and Matthews, 1991).

6. Conclusion

Within a two-layer ocean model, we have shown that GIA bathymetry changes may induce substantial Southern Ocean flow variations. The dominant mechanism causing these flow changes is attributed to the change in the JEBAR effect, which represents the impact of bottom topography on a stratified flow. Locally, however, the vorticity contribution from the eddy stresses is equally strong.

The repositioning of fronts and the changing variability of the velocity can change local nutrient availability, erosion and sedimentation rates, ocean heat transport, mixing, upwelling and downwelling patterns that may eventually affect ice sheet stability, and damp or accentuate other processes used to explain sediment records.

We hope that the results in this paper will stimulate simulations with *coupled* atmosphere–ocean–ice sheet–sediment–solid earth global models to study the importance of the mechanism identified here in the (paleo)climate system.

Acknowledgments

This work was funded by the Netherlands Organization for Scientific Research (NWO), Earth and Life Sciences, through project ALW 802.01.024. The ocean model computations were done on the Cartesius at SURFsara in Amsterdam. Use of the SURFsara computing facilities was sponsored by NWO under the project SH-209-12. We gratefully acknowledge two anonymous reviewers for detailed suggestions and J. Caves for comments on the manuscript.

Appendix A. Ocean model viscosity and resolution

To resolve the Munk boundary layer with thickness δ_M ($\delta_M^3 = \nu/\beta$) at 67°S with at least three grid points, the viscosity ν should be higher than 360 m^2/s. While with this viscosity value, the model does capture baroclinic instability, the eddy kinetic energy is much weaker than that observed today. For the simulations shown above we chose an along isopycnal viscosity of 50 m^2/s, an absolute minimum to represent

a Munk boundary layer. In Table A.1 sensitivity tests are summarized. Different horizontal resolutions (0.25°, 0.5°, and 1°) and viscosities (500, and 0.5 m^2/s) test the impact of interfacial form stress and propagation of numerical errors induced by not fully resolving the Munk boundary layer into the interior of the ocean.

With high viscosity the total transport increases for the same resolution, variability and eddies reduce (rows 1–3). The flow fields (not shown) are very similar to the ones shown in the main text, except for the gyre west of Drake Passage of which the strength is dependent on the baroclinicity of the flow. For low viscosity (last row) locally the flow differs from the higher viscous cases, but the control run structures shift in the same way responding to the GIA bathymetry and sea level reduction as in the other runs. Numerical instabilities seem to play a minor role even at this low viscosity.

As the layer height decreases the Rossby deformation radius decreases and fewer eddies get resolved. Thus, reduction of the upper layer height is more efficient than of the lower layer in reducing the variability of the flow.

Table A.1
25 average Drake Passage transport in Sv (variance). Columns show horizontal resolutions (e.g. 1° × 1°) and viscosity sensitivity experiments. First three rows = control run, next three rows = Glacial Isostatic Adjustment run with upper level depth reduction to simulate sea level drop, next three rows = GIA lower level depth reduction, last three rows = nonmass conserving run with GIA bathymetry but no water column height reduction. Bold runs are shown in the main paper. The variance changes according to the relative layer height.

Run	Layers	1° High visc	0.5° High visc	0.25° High visc	0.25° Med visc	0.25° Low visc
Control	Both	149.58	150.71	149.59 (25)	**125.2** (**95**)	124.4 (47)
	Upper	146.23	142.60	129.90 (9)	**118.6** (**15**)	118.2 (9)
	Lower	3.35	8.11	19.69 (17)	**6.5** (**41**)	6.2 (21)
GIA UL	Both	132.44	132.54	132.35 (12)	**109.8** (**21**)	110.5 (24)
	Upper	129.57	122.55	126.64 (6)	**105** (**5**)	105.5 (5)
	Lower	2.87	9.99	15.72 (10)	**5** (**10**)	5 (11)
GIA LL	Both				117.6 (45)	117.2 (48)
	Upper				115 (10)	115 (11)
	Lower				2.6 (17)	2.2 (18)
GIA non	Both				118 (55)	117.8 (58)
	Upper				115.6 (11)	115.6 (11)
	Lower				2.4 (21)	2.2 (24)

References

Barker, P., Burrell, J., 1977. The opening of Drake Passage. Mar. Geol. 25, 15–34. http://dx.doi.org/10.1016/0025-3227(77)90045-7 (URL: http://www.sciencedirect.com/science/article/pii/0025322777900457).

Barker, P., Thomas, E., 2004. Origin, signature and palaeoclimatic influence of the Antarctic circumpolar current. Earth Sci. Rev. 66, 143–162. http://dx.doi.org/10.1016/j.earscirev.2003.10.003 (URL: http://www.sciencedirect.com/science/article/pii/S0012825203001272).

Bijl, P.K., Bendle, J.A.P., Bohaty, S.M., Pross, J., Schouten, S., Tauxe, L., Stickley, C.E., McKay, R.M., Röl, U., Olney, M.P., Sluijs, A., Escutia, C., Brinkhuis, H., Expedition 318 Scientists, 2013. Eocene cooling linked to early flow across the Tasmanian Gateway. PNAS. http://dx.doi.org/10.1073/pnas.1220872110 (URL: http://www.pnas.org/content/early/2013/05/28/1220872110.abstract).

Cane, M.A., Kamenkovich, V.M., Krupitsky, A., 1998. On the utility and disutility of JEBAR. J. Phys. Oceanogr. 28, 519–526. http://dx.doi.org/10.1175/1520-0485(1998)028<0519:OTUADO>2.0.CO;2 (URL: http://dx.doi.org/10.1175/1520-0485(1998)028<0519:OTUADO>2.0.CO;2).

Close, D.I., Watts, a.B., Stagg, H.M.J., 2009. A marine geophysical study of the Wilkes Land rifted continental margin, Antarctica. Geophys. J. Int. 177, 430–450. http://dx.doi.org/10.1111/j.1365-246X.2008.04066.x (URL: http://doi.wiley.com/10.1111/j.1365-246X.2008.04066.x).

Conrad, C.P., 2013. The solid earth's influence on sea level. Geol. Soc. Am. Bull. 125, 1027–1052. http://dx.doi.org/10.1130/B30764.1 (URL: http://gsabulletin.gsapubs.org/content/125/7-8/1027.abstract).

Cristini, L., Grosfeld, K., Butzin, M., Lohmann, G., 2012. Influence of the opening of the Drake Passage on the Cenozoic Antarctic Ice Sheet: a modeling approach. Palaeogeogr. Palaeoclimatol. Palaeoecol. 339–341, 66–73. http://dx.doi.org/10.1016/j.palaeo.2012.04.02 (URL: http://www.sciencedirect.com/science/article/pii/S0031018212002271).

Dalziel, I., Lawver, L., Pearce, J., Barker, P., Hastie, A., Barfod, D., Schenke, H.W., Davis, M., 2013. A potential barrier to deep Antarctic circumpolar flow until the late Miocene? Geology 41, 947–950. http://dx.doi.org/10.1130/G34352.1 (URL: http://geology.gsapubs.org/content/41/9/947.abstract).

DeConto, R.M., Pollard, D., Wilson, P.A., Palike, H., Lear, C.H., Pagani, M., 2008. Thresholds for Cenozoic bipolar glaciation. Nature 455, 652–656. http://dx.doi.org/10.1038/nature07337.

Diester-Haass, L., Zahn, R., 1996. Eocene–Oligocene transition in the Southern Ocean: history of water mass circulation and biological productivity. Geology 24, 163–166.

Egan, K.E., Rickaby, R.E., Hendry, K.R., Halliday, A.N., 2013. Opening the gateways for diatoms primes Earth for Antarctic glaciation. Earth Planet. Sci. Lett. 375, 34–43. http://dx.doi.org/10.1016/j.epsl.2013.04.030 (URL: http://www.sciencedirect.com/science/article/pii/S0012821X13002185).

Farrell, W.E., Clark, J.A., 1976. On postglacial sea level. Geophys. J. R. Astron. Soc. 46, 647–667. http://dx.doi.org/10.1111/j.1365-246X.1976.tb01252.x (URL: http://dx.doi.org/10.1111/j.1365-246X.1976.tb01252.x).

Gallagher, S.J., Villa, G., Drysdale, R.N., Wade, B.S., Scher, H., Li, Q., Wallace, M.W., Holdgate, G.R., 2013. A near-field sea level record of East Antarctic Ice Sheet instability from 32 to 27 Myr. Paleoceanography. http://dx.doi.org/10.1029/2012PA002326 (URL: http://dx.doi.org/10.1029/2012PA002326).

Goldner, A., Huber, M., Caballero, R., 2013. Does Antarctic glaciation cool the world? Clim. Past 9, 173–189. http://dx.doi.org/10.5194/cp-9-173-2013 (URL: http://www.clim-past.net/9/173/2013/).

Graham, R.M., de Boer, A.M., Heywood, K.J., Chapman, M.R., Stevens, D.P., 2012. Southern ocean fronts: controlled by wind or topography? J. Geophys. Res. 117, C08018. http://dx.doi.org/10.5194/cp-8-1257-2012 (URL: http://dx.doi.org/10.1029/2012JC007887).

Griffies, S.M., Hallberg, R.W., 2000. Biharmonic friction with a Smagorinsky-like viscosity for use in large-scale eddy-permitting ocean models. Mon. Weather Rev. 128, 2935–2946. http://dx.doi.org/10.1175/1520-0493(2000)128<2935:BFWASL>2.0.CO;2 (URL: http://dx.doi.org/10.1175/1520-0493(2000)128<2935:BFWASL>2.0.CO;2).

Hallberg, R., 1997. Stable split time stepping schemes for large-scale ocean modeling. J. Comput. Phys. 135, 54–65 (URL: http://www.sciencedirect.com/science/article/pii/S002199919795734X).

Hambrey, M., Ehrmann, W., Larsen, B., 1991. Cenozoic glacial record of the Prydz Bay continental shelf, East Antarctica. In: Barron, J., Larsen, B.e.a.e (Eds.), Proc. ODP, Sci. Results, College Station, TX. Ocean Drilling Program, vol. 119, pp. 77–132. http://dx.doi.org/10.2973/odp.proc.sr.119.200.1991 (URL: http://dx.doi.org/10.2973/odp.proc.sr.119.200.1991).

Hassold, N.J., Rea, D.K., van der Pluijm, B.A., Parés, J.M., 2009. A physical record of the Antarctic circumpolar current: Late Miocene to recent slowing of abyssal circulation. Palaeogeogr. Palaeoclimatol. Palaeoecol. 275, 28–36. http://dx.doi.org/10.1016/j.palaeo.2009.01.01 (URL: http://www.sciencedirect.com/science/article/pii/S0031018209000315).

Heinze, C., Crowley, T.J., 1997. Sedimentary response to ocean gateway circulation changes. Paleoceanography 12, 742–754. http://dx.doi.org/10.1029/97PA02050 (URL: http://dx.doi.org/10.1029/97PA02050).

Hernández-Molina, F.J., Paterlini, M., Violante, R., Marshall, P., de Isasi, M., Somoza, L., Rebesco, M., 2009. Contourite depositional system on the argentine slope: an exceptional record of the influence of Antarctic water masses. Geology 37, 507–510. http://dx.doi.org/10.1130/G25578A.1 (URL: http://geology.gsapubs.org/content/37/6/507.abstract).

Huber, M., Nof, D., 2006. The ocean circulation in the Southern Hemisphere and its climatic impacts in the Eocene. Palaeogeogr. Palaeoclimatol. Palaeoecol. 231, 9–28. http://dx.doi.org/10.1016/j.palaeo.2005.07.037 (URL: http://www.sciencedirect.com/science/article/pii/S0031018205004785).

Ito, T., Woloszyn, M., Mazloff, M., 2010. Anthropogenic carbon dioxide transport in the Southern Ocean driven by Ekman flow. Nature 463, 80–83. http://dx.doi.org/10.1038/nature08687.

Jr, D.M., Robinson, A., 1997. Eddy-induced nutrient supply and new production in the Sargasso Sea. Deep-Sea Res. I Oceanogr. Res. Pap. 44, 1427–1450. http://dx.doi.org/10.1016/S0967-0637(97)00024-1 (URL: http://www.sciencedirect.com/science/article/pii/S0967063797000241).

Kennett, J.P., 1977. Cenozoic evolution of Antarctic glaciation, the circum-Antarctic Ocean, and their impact on global paleoceanography. J. Geophys. Res. 82, 3843–3860. http://dx.doi.org/10.1029/JC082i027p03843 (URL: http://dx.doi.org/10.1029/JC082i027p03843).

Latimer, J.C., Filippelli, G.M., 2002. Eocene to Miocene terrigenous inputs and export production: geochemical evidence from ODP Leg 177, Site 1090. Palaeogeogr. Palaeoclimatol. Palaeoecol. 182, 151–164. http://dx.doi.org/10.1016/S0031-0182(01)00493- (URL: http://www.sciencedirect.com/science/article/pii/S003101820100493X).

Lawver, L.A., Gahagan, L.M., 2003. Evolution of Cenozoic seaways in the circum-Antarctic region. Palaeogeogr. Palaeoclimatol. Palaeoecol. 198, 11–37. http://dx.doi.org/10.1016/S0031-0182(03)00392-4 (URL: http://www.ingentaconnect.com/content/els/00310182/2003/00000198/00000001/art00392).

Lefebvre, V., Donnadieu, Y., Sepulchre, P., Swingedouw, D., Zhang, Z.S., 2012. Deciphering the role of southern gateways and carbon dioxide on the onset of the Antarctic Circumpolar Current. Paleoceanography. http://dx.doi.org/10.1029/2012PA002345 (URL: http://dx.doi.org/10.1029/2012PA002345).

Livermore, R., Nankivell, A., Eagles, G., Morris, P., 2005. Paleogene opening of Drake Passage. Earth Planet. Sci. Lett. 236, 459–470. http://dx.doi.org/10.1016/j.epsl.2005.03.027 (URL: http://www.sciencedirect.com/science/article/pii/S0012821X05002785).

Markwick, P.J., Rowley, D.B., Ziegler, A.M., Hulver, M.L., Valdes, P.J., Sellwood, B.W., 2000. Late cretaceous and Cenozoic global palaeogeographies: mapping the transition from a "hot-house" to an "ice-house" world. GFF 122, 103. http://dx.doi.org/10.1080/11035890001221103 (URL: http://www.tandfonline.com/doi/abs/10.1080/11035890001221103).

McQuarrie, N., van Hinsbergen, D.J., 2013. Retrodeforming the Arabia–Eurasia collision zone: age of collision versus magnitude of continental subduction. Geology 41, 315–318. http://dx.doi.org/10.1130/G33591.1 (URL: http://geology.gsapubs.org/content/41/3/315.abstract).

Mertz, G., Wright, D.G., 1992. Interpretations of the JEBAR term. J. Phys. Oceanogr. 22, 301–305. http://dx.doi.org/10.1175/1520-0485(1992)022<0301:IOTJT>2.0.CO;2 (URL: http://dx.doi.org/10.1175/1520-0485(1992)022<0301:IOTJT>2.0.CO;2).

Meulenkamp, J.E., Sissingh, W., 2003. Tertiary palaeogeography and tectonostratigraphic evolution of the northern and southern peri-tethys platforms and the intermediate domains of the African–Eurasian convergent plate boundary zone. Palaeogeogr. Palaeoclimatol. Palaeoecol. 196, 209–228. http://dx.doi.org/10.1016/S0031-0182(03)00319- (URL: http://www.sciencedirect.com/science/article/pii/S0031018203003195).

Mitrovica, J.X., Peltier, W.R., 1991. On postglacial geoid subsidence over the equatorial oceans. J. Geophys. Res. Solid Earth 96, 20053–20071. http://dx.doi.org/10.1029/91JB01284 (URL: http://dx.doi.org/10.1029/91JB01284).

Mix, H.T., Mulch, A., Kent-Corson, M.L., Chamberlain, C.P., 2011. Cenozoic migration of topography in the North American Cordillera. Geology 39, 87–90. http://dx.doi.org/10.1130/G31450.1 (URL: http://geology.gsapubs.org/content/39/1/87.abstract).

Müller, R.D., Sdrolias, M., Gaina, C., Roest, W.R., 2008. Age, spreading rates, and spreading asymmetry of the world's ocean crust. Geochem. Geophys. Geosyst. 9, 1525–2027. http://dx.doi.org/10.1029/2007GC001743 (URL: http://dx.doi.org/10.1029/2007GC001743).

Oglesby, R.J., 1989. A GCM study of Antarctic glaciation. Clim. Dyn. 3, 135–156. http://dx.doi.org/10.1007/BF01080365 (URL: http://dx.doi.org/10.1007/BF01080365).

Olbers, D., Brobowski, D., Voelker, C., Woelff, J.O., 2004. The dynamical balance, transport and circulation of the Antarctic circumpolar current. Antarct. Sci. 16, 439–470. http://dx.doi.org/10.1017/S0954102004002251.

Peltier, W.R., 1974. The impulse response of a Maxwell Earth. Rev. Geophys. 12, 649–669. http://dx.doi.org/10.1029/RG012i004p00649 (URL: http://dx.doi.org/10.1029/RG012i004p00649).

Pfuhl, H.A., McCave, I.N., 2005. Evidence for late Oligocene establishment of the Antarctic circumpolar current. Earth Planet. Sci. Lett. 235, 715–728. http://dx.doi.org/10.1016/j.epsl.2005.04.025 (URL: http://www.sciencedirect.com/science/article/pii/S0012821X05002712).

Prentice, M.L., Matthews, R.K., 1991. Tertiary ice sheet dynamics: the snow gun hypothesis. J. Geophys. Res. 96, 6811–6827. http://dx.doi.org/10.1029/90JB01614 (URL: http://dx.doi.org/10.1029/90JB01614).

Sarkisyan, A., Ivanov, V., 1971. Joint effect of baroclinicity and bottom relief as an important factor in the dynamics of sea currents. Izv. Akad. Nauk SSSR, Fiz. Atmos. Okeana 7, 173–188.

Scher, H.D., Martin, E.E., 2006. Timing and climatic consequences of the opening of Drake Passage. Science 312, 428–430. http://dx.doi.org/10.1126/science.1120044 (URL: http://www.sciencemag.org/content/312/5772/428.abstract).

Sijp, W.P., England, M.H., 2011. Effect of the deepening of the Tasman Gateway on the global ocean. Paleoceanography 26, PA4207. http://dx.doi.org/10.1029/2011PA002143 (URL: http://dx.doi.org/10.1029/2011PA002143).

Sluijs, A., et al., 2003. Dinoflagellate cysts from the Eocene–Oligocene transition in the Southern Ocean: results from ODP Leg 189. 189, 1–42.

Smith, C., Richards, K., Fasham, M., 1996. The impact of mesoscale eddies on plankton dynamics in the upper ocean. Deep-Sea Res. I Oceanogr. Res. Pap. 43, 1807–1832. http://dx.doi.org/10.1016/S0967-0637(96)00035-0 (URL: http://www.sciencedirect.com/science/article/pii/S0967063796000350).

Sokolov, S., Rintoul, S.R., 2007. On the relationship between fronts of the Antarctic circumpolar current and surface chlorophyll concentrations in the Southern Ocean. J. Geophys. Res. Oceans 112. http://dx.doi.org/10.1029/2006JC004072 (URL: http://dx.doi.org/10.1029/2006JC004072).

Somme, T.O., Helland-Hansen, W., Granjeon, D., 2009. Impact of eustatic amplitude variations on shelf morphology, sediment dispersal, and sequence stratigraphic interpretation: icehouse versus greenhouse systems. Geology 37, 587–590. http://dx.doi.org/10.1130/G25511A.1 (URL: http://geology.gsapubs.org/cgi/doi/10.1130/G25511A.1).

Spada, G., Stocchi, P., 2007. SELEN: a Fortran 90 program for solving the sea-level equation. Comput. Geosci. 33, 538–562. http://dx.doi.org/10.1016/j.cageo.2006.08.006 (URL: http://www.sciencedirect.com/science/article/pii/S0098300406001786).

Spence, P., Saenko, O.A., Dufour, C.O., Sommer, J.L., England, M.H., 2012. Mechanisms maintaining southern ocean meridional heat transport under projected wind forcing. J. Phys. Oceanogr. http://dx.doi.org/10.1175/JPO-D-12-03.1 (URL: http://dx.doi.org/10.1175/JPO-D-12-03.1).

Stickley, C.E., Brinkhuis, H., Schellenberg, S.A., Sluijs, A., Ruehl, U., Fuller, M., Grauert, M., Huber, M., Warnaar, J., Williams, G.L., 2004. Timing and nature of the deepening of the Tasmanian Gateway. Paleoceanography 19, PA4027. http://dx.doi.org/10.1029/2004PA001022 (URL: http://dx.doi.org/10.1029/2004PA001022).

Stocchi, P., Escutia, C., Houben, A.J.P., Vermeersen, B.L.A., Bijl, P.K., Brinkhuis, H., DeConto, R.M., Galeotti, S., Passchier, S., Pollard, D., Klaus, A., Fehr, A., Williams, T., Bendle, J.A.P., Bijl, P.K., Bohaty, S.M., Carr, S.A., Dunbar, R.B., Flores, J.A., Gonzàlez, J.J., Hayden, T.G., Iwai, M., Jimenez-Espejo, F.J., Katsuki, K., Kong, G.S., McKay, R.M., Nakai, M., Olney, M.P., Pekar, S.F., Pross, J., Riesselman, C., Röhl, U., Sakai, T., Shrivastava, P.K., Stickley, C.E., Sugisaki, S., Tauxe, L., Tuo, S., van de Flierdt, T., Welsh, K., Yamane, M., 2013. Relative sea-level rise around East Antarctica during Oligocene glaciation. Nat. Geosci. 6, 380–384. http://dx.doi.org/10.1038/ngeo1783.

Tigchelaar, M., von der Heydt, A.S., Dijkstra, H.A., 2011. A new mechanism for the two-step $\delta^{18}O$ signal at the Eocene–Oligocene boundary. Clim. Past 7, 235–247. http://dx.doi.org/10.5194/cp-7-235-2011 (URL: http://www.clim-past.net/7/235/2011/).

Torsvik, T.H., van der Voo, R., Preeden, U., Mac, Niocaill C., Steinberger, B., Doubrovine, P.V., van Hinsbergen, D.J.J., Domeier, M., Gaina, C., Tohver, E., Meert, J.G., McCausland, P.J.A., Cocks, L.R.M., 2012. Phanerozoic polar wander, paleogeography and dynamics. Earth Sci. Rev. 114, 325–368. http://dx.doi.org/10.1016/j.earscirev.2012.06.007.

van Hinsbergen, D.J.J., Lippert, P.C., Dupont-Nivet, G., McQuarrie, N., Doubrovine, P.V., Spakman, W., Torsvik, T.H., 2012. Greater India Basin hypothesis and a two-stage Cenozoic collision between India and Asia. Proc. Natl. Acad. Sci. 109. http://dx.doi.org/10.1073/pnas.1117262109 (URL: http://www.pnas.org/cgi/doi/10.1073/pnas.1117262109).

Wilson, D.S., Jamieson, S.S., Barrett, P.J., Leitchenkov, G., Gohl, K., Larter, R.D., 2012. Antarctic topography at the Eocene–Oligocene boundary. Palaeogeogr. Palaeoclimatol. Palaeoecol. 335, 24–34. http://dx.doi.org/10.1016/j.palaeo.2011.05.028 (URL: http://www.sciencedirect.com/science/article/pii/S0031018211002732).

Wilson, D.S., Pollard, D., DeConto, R.M., Jamieson, S.S., Luyendyk, B.P., 2013. Initiation of the West Antarctic Ice Sheet and estimates of total Antarctic ice volume in the earliest Oligocene. Geophys. Res. Lett. http://dx.doi.org/10.1002/grl.50797 (URL: http://dx.doi.org/10.1002/grl.50797).

Yang, S., Galbraith, E., Palter, J., Dynamics, Climate, 2013. Coupled climate impacts of the Drake Passage and the Panama Seaway. Clim. Dyn. 1–16. http://dx.doi.org/10.1007/s00382-013-1809-6 (URL: http://dx.doi.org/10.1007/s00382-013-1809-6).

Zachos, J.C., Flower, B.P., Paul, H., 1997. Orbitally paced climate oscillations across the Oligocene/Miocene boundary. Nature 388, 567–570.

Zambianchi, E., Budillon, G., Falco, P., Spezie, G., 1999. Oceanography of the Ross Sea. chapter Observations of the Dynamics of the Antarctic Circumpolar Current in the Pacific Sector of the Southern OceanSpringer-Verlag, Milan pp. 37–50.